An Exploration of the Temperature of an Accretion Disk Around a Pseudo-Newtonian Black Hole

Jonah Miller
jonah.maxwell.miller@gmail.com

Fundamentals of Astrophysics
Niayesh Afshordi
Fall 2013

Abstract

We attempt to reproduce the work of Shafee et al. in their 2008 paper [1] to measure the temperature of a thin accretion disk. We consider a thin accretion disk around a pseudo-Newtonian stellar black hole. By numerically solving the non-relativistic hydrodynamics equations consistently, and assuming blackbody radiation from the surface, we find the spectrum of the disk.

1 Introduction

Einstein's theory of theory of general relativity predicts the formation of singularities known as black holes [2]. The gravitational pull of a black hole is so strong that, once an object passes within a certain distance, known as the Schwarzschild radius, the object is inexorably pulled into the curvature singularity at the center of the black hole, never to be seen again [2]. One might hope that these black holes are mathematical artifacts that one wouldn't really observe in nature. However, the singularity theorems of Hawking and Ellis demonstrate that, given reasonable assumptions on the makeup of matter in the universe, black holes are plentiful [3].

Indeed, a number of astrophysical black holes have been observed, and their properties measured [4, 5, 6, 7].[1] And although this work will focus on astrophysical black holes, it is believed that every galaxy has a super-massive black hole at its center [8]. A black hole's enormous gravity pulls many objects inwards towards the black hole and these form a disk of accreting matter [7, 9]. It is this "accretion disk" (and the ultra-relativistic jets emerging from the poles of the black hole) that is most visible from Earth [7, 9].

To learn about an astrophysical black hole, we study the properties of the accretion disk and how they are related to the black hole. To do this, we need a reliable, predictive model that relates the black hole parameters[2] to the properties of the accretion disk. The fluid dynamics of accretion disks are extremely complicated. In full generality, one needs to simulate a highly nonlinear system of hyperbolic partial differential equations in (3+1) dimensions [11, 12, 13, 14].[3] However, this is computationally expensive and one can often extract useful data with a much simpler model.

In their 2008 paper, Shafee and collaborators propose one such model [1], which is the continuation of a long history of models [32, 33, 34, 35, 36, 37, 38, 50, 39, 40, 41]. The model uses fluid dynamics and a number of approximations to generate a nonlinear system of ordinary differential equations (ODEs), which must be solved numerically. In an effort to understand this model, and to generate an accessible discussion of accretion disk physics, we present the following attempt to reproduce Shafee et al.'s work. Ultimately, we

[1] This is only a small fraction of the literature on black hole observations.

[2] A black hole only has three possible parameters; mass, charge, and spin. The No-Hair Theorem guarantees that every black hole is completely defined by these three quantities [10].

[3] There are many many more papers to cite here. This is only a sampling.

aren't successful in reproducing the numerical results. However, we effectively reproduce the analytic system that must be solved numerically, and we believe our numerical failure is interesting in its own right.

In section 2, we introduce some key concepts from accretion disk physics that we need to understand Shafee et al.'s model. This includes Keplerian motion, fluid dynamics, and the α prescription of Shakura and Sunyaev. In section 3, we present a derivation of the boundary-value problem that Shafee et al. solve numerically. We discuss the approximation of a black hole using a Pseudo-Newtonian potential. We discuss how the equations of mass, energy, and momentum conservation result in an ODE system that we want to solve. And we discuss how to generate boundary data. In section 4, we discuss our approach to numerically solving Shafee et al.'s ODE system, including methods and tests of our implementation. In section 5 we discuss the results of our numerical simulations and what approach might work better. Finally, in section 6, we offer some concluding remarks.

2 Background

In this section, we will discuss some typical features of accretion disk models, including Keplerian motion, the fluid dynamics required to develop models of accretion disks and the so-called α prescription.

2.1 Keplerian Motion

In the context of accretion disks, Keplerian motion means circular motion. Given an arbitrary spherically symmetric potential Φ, we derive the angular velocity of a circular orbit, also called the "Keplerian angular velocity," here.

Suppose we have a test particle in our potential Φ. Then the acceleration due to gravity on the particle is

$$g = -\vec{\nabla}\Phi\hat{R}, \tag{1}$$

where $\hat{R}$ is the radial direction. However, if the orbit is circular, we know that the centripetal acceleration must be

$$a_c = -R\Omega_K^2, \tag{2}$$

where R is the radius and Ω_K is the Keplerian angular velocity. If we set these quantities equal to each other, we find that

$$\Omega_K = \sqrt{\frac{-\vec{\nabla}\Phi}{R}}\hat{z}, \tag{3}$$

where $\hat{z}$ is perpendicular to the orbital plane.

2.2 Fluid Dynamics

We model accretion disks as fluids orbiting a central compact object, so we must also discus fluid dynamics. In this discussion, we borrow mostly from [9] and [15]. First, let us define the following functions of the radius R:

ρ	is the density of the fluid	(4)
$\vec{v}$	is the velocity field of the fluid	(5)
v_R	is the radial velocity	(6)
P	is the total pressure in the fluid	(7)
c_s	is the speed of sound	(8)
Ω	is the angular velocity	(9)
Ω_K	is the angular velocity for a text particle in a Keplerian orbit	(10)
H	is one half the vertical thickness of the disk.	(11)
$\dot{M}$	is the accretion rate of the black hole.	(12)

The equations of fluid dynamics encode conservation laws. Therefore, we want to discuss the change in time of energy, mass, and momentum. One important issue in formalizing these equations is that we want to discuss the change due to the internal dynamics of the fluid and due to the motion of the fluid as a whole. This leads us to the comoving derivative[4] [15],

$$\frac{D}{Dt} = \frac{\partial}{\partial t} + \vec{v} \cdot \vec{\nabla}. \tag{13}$$

Now, encoded in the language of fluid dynamics, the conservation of mass law, also called the continuity equation, is written as [9, 15]

$$\frac{D\rho}{Dt} + \rho\vec{\nabla} \cdot \vec{v} = 0. \tag{14}$$

The equation of conservation of momentum can be written as

$$\rho\frac{D\vec{v}}{Dt} = -\vec{\nabla}P + \rho\Omega^2\vec{r} + \rho\vec{\nabla} \cdot \sigma, \tag{15}$$

where $\vec{r}$ is the standard position vector and σ is the stress tensor [9, 15, 16]. In this form, equation (15) is just a restatement of Newton's second law. Later, we will see that, just as Newton's second law can be broken into linear and angular parts, this equation can be broken into two pieces, a linear momentum conservation law, and an angular momentum conservation law.

Energy conservation is a little different. We actually have two coupled energy conservation laws: one for mechanical energy and one for thermal energy [9, 15]. The mechanical energy equation is [15]

$$\frac{D}{Dt}\left(\frac{1}{2}\vec{v}^2\right) = -\frac{1}{\rho}\vec{v} \cdot \vec{\nabla}P + \vec{v} \cdot \vec{f}. \tag{16}$$

This just tells us that the rate of change of kinetic energy per unit volume is the same as the work done per unit volume on the fluid. The thermal energy equation is written as

$$\frac{DU}{Dt} = \frac{P}{\rho^2}\frac{D\rho}{Dt} + q^+ - q^- - \frac{1}{\rho}\vec{\nabla} \cdot (k\vec{\nabla}T), \tag{17}$$

where U is the internal energy per unit volume, q^+ and q^- are the rates of heating and cooling in the fluid, most often generated by viscosity and radiation respectively, k is the thermal conductivity of the fluid, and T is the internal temperature. Therefore, the last term is the heat flux out of a unit volume of fluid [15, 17]. We can also write equation (17) in terms of the entropy per unit mass s [1]

$$\rho T\frac{Ds}{Dt} = q^+ + q^- = fq^+, \tag{18}$$

where

$$f = 1 - \frac{q^-}{q^+}. \tag{19}$$

To solve these equations, one typically adds a relationship between density and pressure, called an equation of state. The speed of sound is usually defined as the adiabatic derivative

$$c_s^2 = \left(\frac{d\rho}{dP}\right)_s, \tag{20}$$

where s is constant [15, 18].

In the case of accretion disks, we will limit ourselves to the following reasonable equation of state [1, 7, 9]

$$P = \rho c_s^2. \tag{21}$$

Note that this is equivalent to assuming the bulk modulus is equal to the total pressure and using the Newton-Laplace equation to define the speed of sound [18].

[4] Also called the Lagrangian derivative

2.3 The Problem of Angular Momentum Transport

Now, let's talk about our fluid orbiting a Newtonian black hole. (We will substantially weaken this assumption later.) In the following discussion, we follow mostly [7] and [9]. However, the original derivation is by Shakura and Sunyaev [19].

Our first task is to describe how our black hole eats. In-falling matter was most likely captured traveling tangential to the black hole, not right towards it. This means that, in the center of mass frame (essentially the frame of the black hole), the in-falling matter carries angular momentum. Over time, may collisions with other in-falling matter will cause the an in-falling particle to lose vertical velocity, but the angular momentum to remains. Figure 1 shows the path of one such in-falling particle. The particle passes the black hole with a velocity vector tangent to it (red), so that in the frame of the black hole, the particle carries angular momentum (blue). However, the black hole's gravitational pull (green) captures the particle, which enters an off-axis, elliptical orbit. Over time, collisions with other in-falling matter will remove the vertical component of the momentum of the particle, but the angular momentum is conserved.

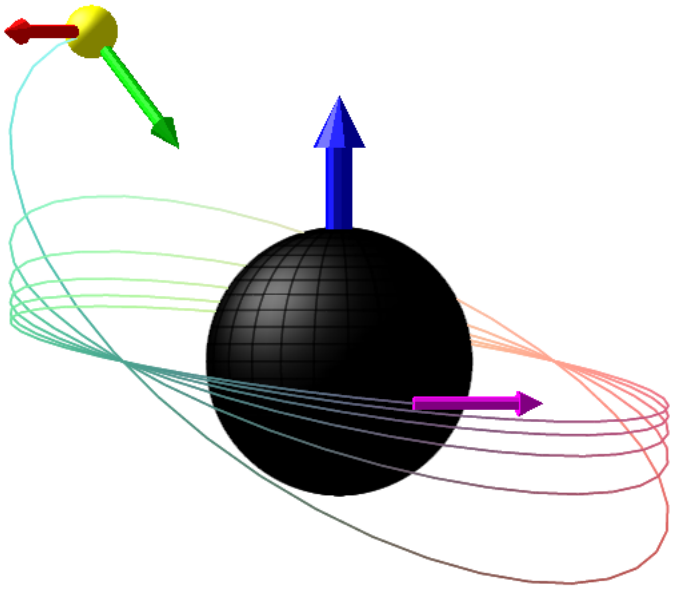

Figure 1: Capture of an in-falling particle by a black hole. The particle passes the black hole with initial velocity tangent to the black hole (red). In the rest frame of the black hole, the particle carries angular momentum (blue). However, the acceleration due to the black hole's gravitational field (green) pulls the particle into an off-axis elliptical orbit. Over time, collisions with other in-falling particles circularize the orbit and remove the vertical component of the particle's velocity, leaving only the tangential in-plane velocity (purple). But the angular momentum remains.

However, if every particle in the disk possesses sufficient angular momentum, then the black hole cannot feed. To see this, we write the energy of a particle as a function of radius, angular momentum, and radial velocity of the particle,

$$E = \frac{1}{2}m\vec{v}^2 - \frac{GMm}{R} \tag{22}$$

$$= \frac{1}{2}mv_R^2 - \frac{GMm}{R} + \frac{L^2}{2I} \tag{23}$$

$$\sim \frac{1}{2}mv_R^2 - \frac{GMm}{R} + \frac{L^2}{R^2}. \tag{24}$$

where M is the mass of the black hole, m is the mass of the particle, $\vec{v}$ is the velocity of the particle, v_R is the radial velocity of the particle, I is the moment of inertia of the particle, L is the angular momentum of the particle, and R is the radius [20].[5]

Since the latter two terms are functions only of R, not its conjugate variables, we can write them together as an "effective potential." Then the energy is the sum of the radial kinetic part and the effective potential parts. If we plot the effective potential, as in figure 2, we find that it diverges as $R \to 0$. This means that a particle needs an infinite radial kinetic energy to reach the origin. For the black hole to eat, it must find some mechanism to deplete the angular momentum of particles nearest the event horizon.

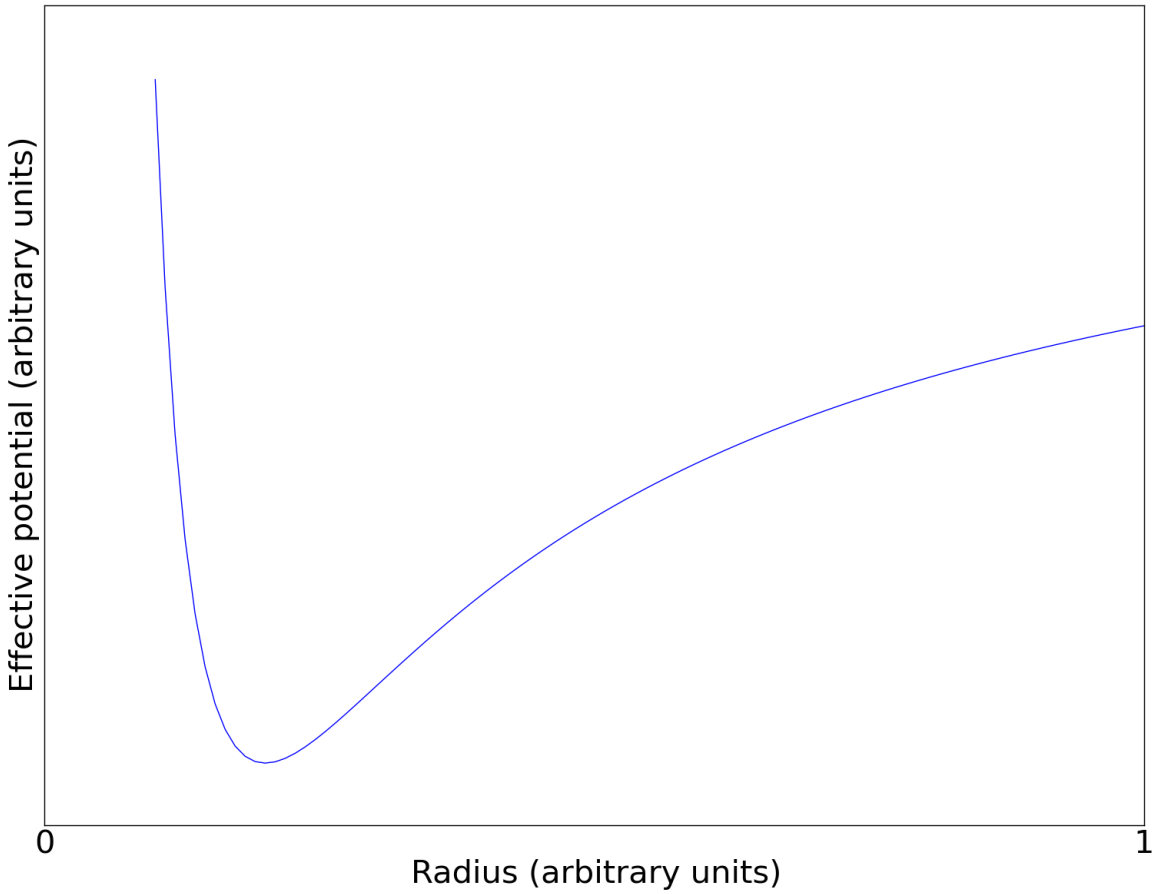

Figure 2: The effective potential of a particle in a rotating reference frame. The potential diverges as the radius approaches zero.

So what is the mechanism behind the angular momentum transfer? If slower moving particles exerted a "drag" force on faster-moving particles, we could get the effect we need. The Keplerian angular velocity of a particle is inversely proportional to the radius, so particles closer in are moving faster, and they would feel a drag torque due to the particles further out. This torque would allow angular momentum to be transferred radially outwards as mass and energy were transferred radially inward [7, 9, 19].

Viscosity exerts a force that suits our needs. However, astrophysical fluids do not have strong enough inter-particle interactions to justify viscosity [8, 9, 19]. Therefore, we need an effective viscosity that fills the

[5]We assume a Newtonian black hole here, but the same intuition holds in the case of a pseudo-Newtonian black hole too.

same role in the stress tensor in equation (15).

Shakura and Sunyaev proposed that the a shear stress—and thus angular momentum transport—could be caused by turbulent motion in the particles in the disk [19], although didn't propose a source for this turbulence. Balbus and Hawley proposed the magneto-rotational instability (MRI) as a source for this turbulence [21, 22, 23, 24, 25], and numerical simulations seem to demonstrate that an effective viscosity is induced by turbulence due to magnetic fields [9, 11, 13, 14, 26, 27].

It is worth noting that this is not the only possible source of angular momentum transport in a disk. It is possible, for instance, that radially-dependent magnetic fields could create a "magnetic pressure" which non-locally transports angular momentum in the appropriate way [7, 8, 19]. Shakura and Sunyaev originally included magnetic pressure in their calculation, and we can likely safely treat it as included in the α prescription described below [19].

2.4 The Alpha Prescription

We now describe how Shakura and Sunyaev use turbulent motion to attain a shear viscosity [7, 9, 19]. As we discussed in section 2.3, orbits in the accretion disk tend to circularize. If they are around a Newtonian black hole with the standard $1/R^2$ potential, the orbits will be Keplerian [7, 9, 19]. Let's consider two neighboring rings of fluid in the accretion disk which follow such orbits. Call them ring A and ring B. Let ring A be at radius R with angular velocity $\Omega(R)$ and let ring B be at radius $R+\lambda$ with angular velocity $\Omega(R+\lambda)$, as shown in figure 3.

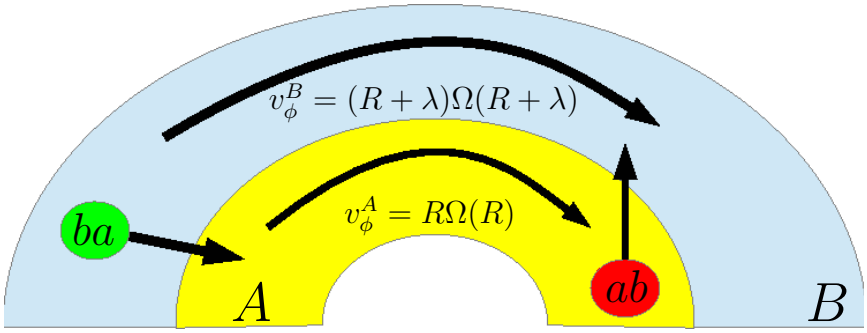

Figure 3: Turbulence as shear viscosity. Two rings in the accretion disk near radius R. A clump of matter from ring A moves to B. Call it ab. Because the fluid is in equilibrium, at the same time, a clump of matter from ring B moves to ring A. Call it ba. Ring A moves with azimuthal velocity $v_\phi^A = R\Omega(R)$. Ring B moves with azimuthal velocity $v_\phi^B = (R+\lambda\Omega(R+\lambda)$. Image inspired by those in [7, 9].

Because of turbulence, clumps of fluid travel between the rings at random, each one carrying angular momentum. Since the fluid is in local hydrodynamic equilibrium, the net flow of clumps is zero—there are as many clumps moving radially outward as there are moving radially inward [7, 9]. Each clump travels a distance of approximately λ at a radial speed of $\tilde{v}$. Each clump has a tangential velocity equal to its radius times its angular velocity. Let's consider two such clumps. One going from ring A to ring B, call it ab and one going from ring B to ring A, call it ba. ab has tangential velocity $v_\phi^A = R\Omega(R)$ and ba has tangential velocity $v_\phi^B = (R+\lambda)\Omega(R+\lambda)$ [7, 9].

As a simplifying assumption, we let the tangential linear angular momentum be conserved.[6] Then the tangential linear momentum flux per unit arc length at a constant radius $R+\lambda/2$ in the outward direction

[6] If we had instead allowed the angular momentum to be conserved, we still would get angular momentum transport radially outward, which is what we want [7].

is [7]

$$\begin{aligned}\Phi_\phi^{AB} &= 2\rho\tilde{v}H(R+\lambda)v_\phi^A \\ &= 2\rho\tilde{V}H(R+\lambda)R\Omega(R),\end{aligned} \tag{25}$$

where H is the height of the disk, as in equation (12). Similarly, the inward flux is [7]

$$\Phi_\phi^{BA} = 2\rho\tilde{v}HR(R+\lambda)\Omega(R+\lambda). \tag{26}$$

Thus the torque on the outer ring by the inward ring is given by the net (outward) flux, which we can approximate as the sum of equations (25) and (26). In the small λ limit, the difference in angular momenta becomes a derivative and we get [7, 9]

$$\tau_{AB} = -\rho\tilde{v}H\lambda R^2\frac{d\Omega(R)}{dR}. \tag{27}$$

Notice that the torque goes to zero in the case of rigid motion where $\frac{d\Omega}{dR}$ is zero. Furthermore, if the angular velocity decreases radially, then the torque outward is positive, transporting angular momentum radially outward [9]. These are the limits we want.

Then the azimuthal shear stress, or the force in the azimuthal direction per unit area:

$$T_\phi = \rho\tilde{v}\lambda R\frac{d\Omega(R)}{dR}. \tag{28}$$

Or, the only non-zero component of the stress tensor is the radial-azimuthal component.

$$\sigma_{R\phi} = \rho\tilde{v}\lambda R\frac{d\Omega(R)}{dR}. \tag{29}$$

We don't know the details of λ or $\tilde{v}$, so we must make some guesses. The motion of the clumps comes from turbulence, and the turbulent eddies are unlikely to be larger than the disk height. So we know [7, 9]

$$\lambda \leq H. \tag{30}$$

Similarly, it is unlikely that the clumps are moving greater than the speed of sound. So we know that [7, 9]

$$\tilde{v} \leq c_s. \tag{31}$$

We then parametrize our lack of knowledge about λ and $\tilde{v}$ by the parameter $\alpha \in [0, 1]$ [7, 9]

$$\sigma_{R\phi} = \alpha\rho c_s HR\frac{d\Omega(R)}{dR}. \tag{32}$$

This is the famous α prescription of Shakura and Sunyaev [19]. It's important to note, however, that we've simply hidden what we don't know inside the α parameter, which we determine numerically. We haven't explained what α should be [7, 9]. In the language of mechanical viscosity, this description becomes

$$\nu = \tilde{v}\lambda = \alpha c_s H. \tag{33}$$

Shakura and Sunyaev actually took this a little further. They argued that the azimuthal velocity is approximately constant and thus

$$\frac{d\Omega}{dR} \approx -\frac{1}{R}\Omega. \tag{34}$$

This isn't as crazy as it sounds, since it is approximately true in the Keplerian case [19, 20]. Now, in the case of a Newtonian potential, it is easy to show that, up to factors of order 1,

$$H = \frac{c_s}{\Omega_K} \tag{35}$$

(see appendix A). If the orbits are all Keplerian anyway, then

$$H = \frac{c_s}{\Omega}$$

and we can use equations (34) and (32) to find

$$\sigma_{R\phi} = -\alpha\rho c_s^2. \tag{36}$$

Or, if we use equation (21) [1],

$$\sigma_{R\phi} = -\alpha P. \tag{37}$$

2.5 Radiation

Let's return to the outward torque we calculated in section 2.4. The torque is radius dependent, so we can write [7, 9]

$$\tau_{out}(R) - \tau_{out}(R + dR) = -\frac{d\tau_{out}}{dR}dR, \tag{38}$$

where τ_{out} is just τ_{AB} from equation (27) rewritten with α,

$$\tau_{out}(R) = -\alpha\rho c_s H^2 R^2 \frac{d\Omega(R)}{dR}. \tag{39}$$

Then the power dissipated by this infinitesimal torque is [7, 9]

$$P = -\Omega\frac{d\tau_{out}}{dR}dR. \tag{40}$$

But by the product rule,

$$\frac{d}{dR}(\tau_{out}\Omega) = \Omega\frac{d\tau_{out}}{dR} + \tau\frac{d\Omega}{dR}. \tag{41}$$

So [9],

$$P = -\left[\frac{d}{dR}(\tau_{out}\Omega) - \tau_{out}\frac{d\Omega}{dR}\right]dR. \tag{42}$$

The first term gives the transfer of rotational energy from the inner radius of the disk to the outer radius of the disk [9]. If we integrate this term, we simply get the difference in rotational energy between the inner-most ring at R_{inner} and the outer ring at R_{outer} [9]:

$$\int_{R_{inner}}^{R_{outer}} \frac{d}{dR}(\tau_{out}\Omega)dR = \tau_{out}\Omega\Big|_{R_{outer}} - \tau_{out}\Omega\Big|_{R_{inner}}. \tag{43}$$

The other term, however, represents the local dissipation of energy into heat [9]. Ultimately, this energy will be radiated by the upper and lower faces of the disk, so in anticipation of a luminosity calculation, we define the energy dissipated per time per unit plane area. Each ring of the disk is at radius R with circumference $2\pi R$ and width d. And it has two surfaces. So we have a unit plane area of

$$4\pi R dR \tag{44}$$

and dissipated energy per unit area per time of [7, 9]

$$D(R) = \frac{\tau_{out}}{4\pi R}\frac{d\Omega}{dR}. \tag{45}$$

The luminosity per unit area at a given radius will be defined by the cooling rate of the fluid (see equation (19)) times $D(R)$ [1]:

$$j^*(R) = (1 - f)D(R). \tag{46}$$

We can use the Stefan-Boltzmann law to solve for the "effective temperature" of the disk at a given radius:

$$j^*(R) = \sigma_B T^4(R) \text{ with } \sigma_B = \frac{2\pi^5 k_B}{15c^2h^3}, \tag{47}$$

where k_B is Boltzmann's constant, c is the speed of light in vacuum, and h is Planck's constant [9]. If we assume blackbody radiation, this gives us the radiated spectrum at a given temperature. The intensity of a given frequency ν is [28]

$$I(\nu, R) = \frac{2h\nu^3}{c^2} \frac{1}{e^{h\nu} k_B T(R) - 1}. \tag{48}$$

And, if we want the observed intensity, we average over every radius and adjust the normalization for distance D_{EBH} and viewing angle i [1]:

$$F(\nu) = \frac{2\pi \cos(i)}{D_{EBH}^2} \int_{R_{inner}}^{R_{outer}} \frac{2h\nu^3 R}{c^2 e^{h\nu/k_B T(R)} - 1} dR. \tag{49}$$

3 The Shafee Model

Now we want to use the tools of section 2 to model a quasi-realistic accretion disk, where the fluid flow can go from subsonic velocities to supersonic velocities.

In the standard approach, one can find the inner-most stable circular orbit (ISCO) around a fully-relativistic fixed Schwarzschild or Kerr black hole[7] and assume that the viscous torque, angular momentum loss, and energy dissipation are all zero within the ISCO [29, 30, 4, 31]. From there one can use the hydrodynamics equations and a wide variety of boundary conditions to solve for the properties of an axisymmetric thin disk.

To test whether or not it is valid to assume these boundary conditions at the ISCO, Shafee et al. developed a pseudo-Newtonian model that still captures some of the relativistic flavor and all of the trans-sonic flavor. The following analytic model of thin accretion disks was pioneered by Paczynski and Bisnovatyi-Kogan [32] and developed by many others [1, 33, 34, 35, 36, 37, 38, 39, 40, 41]. It is less accurate than a fully relativistic simulation, but it is more accurate than the standard thin disk model [1]. Since we are reproducing their results, we primary follow the treatment of Shafee et al. [1] who were in turn guided by Narayan et al. [39].

3.1 The Pseudo-Newtonian Black Hole

Because we want to avoid the extreme computational cost of a fully relativistic magnetohydrodynamics simulation, we will study a simple viscous fluid in a Newtonian gravitational potential. The standard disk model assumes the existence of an ISCO, and we would like to make contact with this notion. For that reason, we use a pseudo-Newtonian gravitational potential, which posses such a radius.

Before we proceed, it is convenient to define the following quantities. Let

$$R_g = \frac{GM}{c^2} \text{ is twice the Schwarzschild radius of the black hole} \tag{50}$$

$$\text{and } a_* = \frac{Jc}{GM^2} \text{ s.t. } -1 < a_* < 1 \text{ is the dimensional spin of the black hole,} \tag{51}$$

where M is the mass of the black hole, J is the spin of the black hole, c is the speed of light, and G is Newton's constant.[8]

[7] It is perhaps a surprising feature of black holes that they can have an inner-most stable circular orbit outside of the event horizon [9, 2].

[8] We can write the spin of the black hole in mass-energy terms as $a = a_* M$ [1].

So that we may include spin, we use Mukhopadhyay's pseduo-Kerr proposal [42], where the acceleration due to gravity of a test particle in a Keplerian orbit at a distance R from the black hole singularity is[9]

$$g = -\vec{\nabla}\Phi = \frac{c^4}{GM}\frac{\left(r^2 - 2a_*\sqrt{r} + a_*^2\right)^2}{r^2\left(\sqrt{r}(r-2) + a_*\right)^2}, \tag{52}$$

where Φ is the gravitational potential and $r = R/R_g$.

When we work with the fluid dynamics, we will hide the effects of gravity in the Keplerian angular velocity at a given radius. (See section 2.1.) In Mukhopadhyay's model, this is [1]:

$$\Omega_K = \frac{c^3}{GM}\frac{(r^2 - 2a_*\sqrt{r} + a_*^2)}{r^2\left(\sqrt{r}(r-2) + a_*\right)}. \tag{53}$$

In the case that $a_* = 0$, the Keplerian angular velocity reduces to

$$\Omega_k = \frac{1}{R - 2R_g}\sqrt{\frac{GM}{R}}. \tag{54}$$

This is the Keplerian angular velocity associated with the gravitational potential proposed by Paczynski and Wiita, also known as the PW80 potential [43]:

$$\Phi = -\frac{GM}{R - 2R_g}. \tag{55}$$

We won't need equations (52) or (55). All the information we need will be contained in equations (53) and (54).

3.2 The Accreting Fluid

To avoid the complexities of (3+1)-dimensional fluid dynamics, we assume axisymmetry and hydrostatic equilibrium for the fluid in the accretion disk. These assumptions are obviously not accurate, however more general simulations and some observational evidence suggest that in the case of a very thin disk, they are often good enough [30, 4, 5, 6, 44, 45].

Since we are assuming hydrostatic equilibrium, the co-moving derivative operator (13) takes an especially simple form:

$$\frac{D}{Dt} = \frac{\partial}{\partial t} + \vec{v}\cdot\vec{\nabla} = v_R\frac{d}{dR}, \tag{56}$$

where t is time [1]. We also assume the α prescription of of Shakura and Sunyaev [19], specifically in the form of equation (37) so that the only component of the viscous stress tensor is the radial-azimuthal shear stress, which is proportional to the pressure. Similarly, as a simplifying assumption we assume that the height is approximately the speed of sound divided by the Keplerian angular velocity as in equation (35).

Now we will endeavor to solve the equations of hydrodynamics, which consist of a mass conservation equation (14), a momentum conservation equation (15), and an energy conservation equation, which we will write as an entropy conservation equation (18).

Between radii R and $R + \Delta R$, the mass is [9]

$$\text{mass} = 4\pi R\rho H dR. \tag{57}$$

If we differentiate this equation with respect to time, we find that [9]

$$R\frac{d4\pi\rho H}{dt} + \frac{d}{dR}\left(4\pi R\rho H v_R\right) = 0. \tag{58}$$

[9]We are writing all of the following formulas in the notation of [1].

And, since we are in a steady state, we find that

$$\frac{d}{dR}\left(4\pi R\rho H v_R\right) = 0. \tag{59}$$

If we integrate, we find that $-\pi R\rho H v_R$ is conserved with respect to the radius. We call this quantity our accretion rate, $\dot{M}$ such that

$$\dot{M} = -4\pi\rho v_R RH = \text{ constant}. \tag{60}$$

This is the integrated form of the continuity equation defined in equation (14) [1, 9].

With the assumptions of axisymmetry, stead-state, and equations With the addition of equations (3), (21), (35) and (37), we can break the momentum conservation equation (equation (15)) into a radial part and an azimuthal part. The radial part becomes [1]

$$v_R\frac{dv_R}{dR} = -(\Omega_K^2 - \Omega^2)R - \frac{1}{\rho}\frac{d}{dR}(\rho c_s^2). \tag{61}$$

Rather than look at the azimuthal part, we impose conservation of angular momentum directly to find that [1]

$$\frac{\rho v_R}{R}\frac{d}{dR}(\Omega R^2) = \frac{1}{R^2 H}\frac{dd(R^2 H\sigma_{R\phi})}{ddR}, \tag{62}$$

where ΩR^2 is the angular momentum per unit mass of the disk at a given radius. This equation can be integrated to find that

$$j = \Omega R^2 + \frac{\alpha c_s^2 R}{v_R}, \tag{63}$$

where j is an integration constant [1].

To adapt the entropy equation (equation (18)) to our needs, we recall that the heating of the gas is due to viscous dissipation (see equation (45)). This gives us that

$$\rho T\frac{Ds}{Dt} = -f\alpha\rho c_s^2 R\frac{d\Omega}{dR}, \tag{64}$$

where here we used equations (20) and (39) [1].

Now we want to set the right-hand side of equation (64) equal to the change in entropy of a comoving clump of gas in the disk. To study our comoving clump of gas, we keep the mass of the gas fixed but allow the other thermodynamic quantities to vary. We will use the fundamental thermodynamic relation

$$dU = TdS - PdV, \tag{65}$$

where U is the internal energy of the system, S is the entropy of the system, and V is the volume [46]. If we reformulate this in the context of fluid dynamics, we have

$$\rho T\frac{Ds}{Dt} = \frac{D\epsilon}{Dt} + \frac{P}{V}\frac{DV}{Dt}, \tag{66}$$

where ϵ is the energy per unit volume and s is the entropy per unit mass (also called specific entropy).

Let's look at the right-most term first. Because of equation (56), we have that

$$\frac{P}{V}\frac{DV}{Dt} = v_R\frac{P}{V}\frac{dV}{dR}. \tag{67}$$

Now, because mass is held fixed, we can write a relationship between $\frac{d\rho}{dR}$ and $\frac{dV}{dR}$:

$$\begin{aligned} \frac{d\rho}{dR} &= \mu\frac{d}{dR}V^{-1} \\ &= -\mu V^{-2}\frac{dV}{dR} \\ \Rightarrow \frac{1}{V}\frac{dV}{dR} &= -\frac{1}{\rho}\frac{d\rho}{dR}, \end{aligned} \tag{68}$$

where μ is the mass of the clump of gas. So, if we also use equation (21), equation (67) becomes

$$\frac{P}{V}\frac{DV}{Dt} = -c_s^2 v_R \frac{d\rho}{dR}. \tag{69}$$

Now let's look at the $\frac{D\epsilon}{Dt}$ term in equation (66). This term should be independent of the volume, so we hold both mass and volume fixed. If we assume the ideal gas law for our fluid,

$$PV = Nk_BT, \tag{70}$$

where V is volume and N is the number of molecules [46], and we assume our gas has an adiabatic index γ,[10] then at a constant volume V, the heat capacity is

$$C_V = \frac{NK_B}{\gamma - 1}, \tag{71}$$

and the thermal energy per unit volume is

$$\epsilon = \frac{C_V T}{V} = \frac{P}{\gamma - 1}. \tag{72}$$

So,

$$\frac{D\epsilon}{Dt} = \frac{v_R}{\gamma - 1}\left(\rho\frac{dc_s^2}{dR} + c_s^2\frac{d\rho}{dR}\right). \tag{73}$$

However, with mass and volume fixed, $\frac{d\rho}{dR} = 0$ and we have that

$$\frac{D\epsilon}{Dt} = \frac{v_R\rho}{\gamma - 1}\frac{dc_s^2}{dR}. \tag{74}$$

Now we can combine equations (66), (69) and (74) to get the change in entropy for a clump of gas in the disk of fixed mass [1, 39]:

$$\rho T\frac{Ds}{Dt} = \frac{\rho v_R}{\gamma - 1}\frac{dc_s^2}{dR} - c_s^2 v_R\frac{d\rho}{dR}. \tag{75}$$

And, finally, we set equations (64) and (75) equal to each other and we find the energy conservation equation for Shafee et al.'s model [1]:

$$\frac{\rho v_R}{\gamma - 1}\frac{dc_s^2}{dR} - c_s^2 v_R\frac{d\rho}{dR} = -f\alpha\rho c_s^2 R\frac{d\Omega}{dR}. \tag{76}$$

3.3 The First-Order ODE System

Other than boundary conditions, we've now written down all the ingredients of Shafee et al.'s model. It would be convenient to reduce the numerous equations we have to a system of ODES to solve for just a few functions of R. We use the definitions of the speed of sound (21) and H (35) and the continuity equation (60) to reduce the variables in the radial (61) and angular (62) momentum and energy equations (76) to just R and three functions of R: v_R, c_s^2, and Ω. We find that

$$\frac{d}{dR}v_R = \frac{v_R}{2\Gamma}\left[\Omega_K\left(3(\gamma-1)\chi + 2c_s^2\Sigma - v_R^2 L(\gamma+1)\right) - 2Rc_s^2\Omega_k'\left(f\alpha^2 c_s^2(\gamma-1) - v_R^2\gamma\right)\right] \tag{77}$$

$$\frac{d}{dR}c_s^2 = \frac{(\gamma-1)c_s^2}{\Gamma}\left[\Omega_K\left(2\chi + f\psi\left(\alpha L + 2Rv_R\Omega - \alpha v_R^2\right) + v_R^2\Xi\right) - R\Omega_K'\left(\chi + v_R^4\right)\right] \tag{78}$$

$$\frac{d}{dR}\Omega = -\frac{v_R}{2\Gamma R}\left[\Omega_K\left(4\alpha(c_s^2)^2\gamma + c_s^2\Lambda - 2Rv_R^3\Omega(\gamma+1)\right) - 2\alpha Rc_s^2\Omega_K'\left(\gamma c_s^2 + v_R^2(\gamma-1)\right)\right] \tag{79}$$

[10] We follow Shafee et al. and assume $\gamma = 3/2$ [1].

with

$$\psi = \alpha c_s^2 \tag{80}$$
$$\chi = f\psi^2 \tag{81}$$
$$L = R^2\left(\Omega^2 - \Omega_K^2\right) \tag{82}$$
$$\Xi = v_R^2 - 2f\alpha R v_R \Omega + L \tag{83}$$
$$\Sigma = f\alpha R\Omega v_R(\gamma - 1) - v_R^2\gamma - f\alpha^2(\gamma - 1)L \tag{84}$$
$$\Lambda = \alpha v_R^2(\gamma - 3) + 4R\Omega v_R\gamma + \alpha L\left(3\gamma - 1\right) \tag{85}$$
$$\Gamma = \frac{1}{2}R\Omega_K\left[2v_R^2\left(f\alpha^2(\gamma - 1) + \gamma\right) - \chi(\gamma - 1) - v_R^4(\gamma + 1)\right] \tag{86}$$

where Ω_K as a function of R is given by equation (53) and we can easily find $\Omega_K' = \frac{d}{dR}\Omega_K$ by differentiating Ω_K.

Note that if we write

$$\vec{y}(R) = \begin{bmatrix} v_R(R) \\ c_s^2(R) \\ \Omega(R) \end{bmatrix}, \tag{87}$$

then we can rewrite our ODE system as a single vector-valued ODE

$$\frac{d}{dR}\vec{y} = \vec{O}(y, R), \tag{88}$$

for the appropriate vector-valued function $\vec{O}$.

3.4 Boundary Conditions and the Shooting Method

We now have a system of three coupled first-order ODEs and three unknown functions of one variable. To solve the system we need the following:

- A length scale. Over what range of R do we wish to solve the system?
- Boundary data. We need three boundary conditions to completely specify the system.

It turns that these two issues are intimately related. Ultimately, we want to study the disk from the Schwarzschild radius to the edge of the disk. However, if we allow spherically-symmetric (Bondi) accretion to inform our intuition, we should expect fluids far from the black hole to have speeds less than the speed of sound and fluids near the black hole to have speeds exceeding the speed of sound [7, 8, 9].

The point where the fluid speed exceeds the sound speed is called the sonic point, R_s, and we should expect our ODE system to become degenerate at this point [1, 7, 8, 9, 39]. To deal with this issue, we will impose regularity conditions that force our ODE system to be well-behaved at the sonic point and use this as boundary data. We can then numerically integrate equations (77), (78), and (79) inward from the boundary of the disk to the sonic point. At the sonic point, we check to insure the regularization conditions hold. If they do, we continue to integrate to the Schwarzschild radius. [1].

There's only one hangup. We don't know where the sonic point *is*. To solve this problem, we use some clever guesswork. We guess a value for R_s and integrate inward to it. If the values of v_R, c_s^2, and Ω at R_s match the regularization conditions, then R_s is the correct sonic point. We can now integrate inwards to the Schwarzschild radius to find the full solution. Otherwise, we cleverly guess a new value for R_s and try again. This is called the *shooting method* [47, 48].

3.4.1 The Self-Similar Solution

Let's talk about the boundary data at the outer boundary of the disk. Since the gravitational potential disappears far from the black hole, it's reasonable to guess that the accretion flow would asymptote to some

uniform behavior far from the black hole. In 1987, Spruit et al. described a set of self-similar solutions for accretion disks while studying shocks in the disk [49]. In 1994, Narayan and Yi rediscovered this solution family. In 1997, Narayan et al. found numerically that, far from the disk, solutions do indeed tend to be self-similar [39].

Assume that

$$\rho = aR^{-3/2},\ v_R = bR^{-1/2},\ \Omega = cR^{-3/2},\ \text{and}\ c_s^2 = dR^{-1}, \tag{89}$$

where a, b, c, and d are constants [50]. Plug this ansatz into the accretion flow equations (77), (78), and (79), and solve for a, b, c, and d. Shafee et al. followed this procedure and found the following self-similar solution [1]:[11]

$$c_{s,ss}^2(R) = c_s^2 \frac{GM}{R} \text{ where } c_0^2 = \frac{2\epsilon'}{5\epsilon' + 2(\epsilon')^2 + \alpha^2} \text{ and } \epsilon' = \frac{5/3 - \gamma}{f(\gamma - 1)}, \tag{90}$$

$$v_{R,ss}(R) = v_0 \sqrt{\frac{GM}{R}},\ \text{where } v_0 = -\alpha \sqrt{\frac{c_0^2}{\epsilon'}}, \tag{91}$$

$$\Omega_{ss}(R) = \Omega_0 \Omega_K(R),\ \text{where } \Omega_0 = \sqrt{c_0^2 \epsilon_0}. \tag{92}$$

It is easy to reproduce this calculation in just a few lines in the likes of Maple or Mathematica.

Because Narayan et al. demonstrated that solutions tend to become self similar [39], rather than solving for the boundary conditions at the edge of the disk, we simply force the solution to be self-similar far away from the sonic point. We call the outer boundary of our computational domain R_{out} and set it equal to

$$R_{out} = 10^5 R_s. \tag{93}$$

Then we have the following outer boundary conditions:

$$v_R(R_{out}) = v_0 \sqrt{\frac{GM}{R_{out}}} \tag{94}$$

$$c_s^2(R_{out}) = c_0^2 \frac{GM}{R_{out}} \tag{95}$$

$$\Omega(R_{out}) = \Omega_0 \Omega_K. \tag{96}$$

3.4.2 Asymptotic Disk Thickness

Before we continue to the conditions at the sonic point, we take a brief detour to discus the asymptotic behavior of the thickness of the disk. Asymptotically,

$$\Omega_K = \sqrt{\frac{GM}{R}}. \tag{97}$$

And so [1]

$$H = \frac{c_{s,ss}}{\Omega_K} = c_0 R$$

$$\Rightarrow \frac{H}{R} = \sqrt{2} \left(5 + 2\, \frac{5/3 - \gamma}{f\,(\gamma - 1)} + \frac{\alpha^2 f\,(\gamma - 1)}{5/3 - \gamma} \right)^{-1/2}. \tag{98}$$

This means that we can set the asymptotic height scale of the disk by setting f [1]. As we will see numerically, the height scale does not change dramatically over most of the disk, so we can enforce that we have a thin disk [1]. For $\gamma = 1.5$, $f = 3.5 \times 10^{-3}$ gives $H/R = 0.1$ and $f = 3.5 \times 10^{-5}$ gives $H/R = 0.01$. We choose $H/R = 0.01$, which enforces an extremely thin dramatically radiation-cooled disk.

[11] We follow Shafee et al.'s lead and use the "ss" subscript to mean "self-similar" [1].

3.4.3 Regularizing the Sonic Point

When $\|\vec{v}\| = \sqrt{\left(v_R\hat{R} + R\Omega(R)\hat{\phi}\right)^2}$ becomes equal to c_s^2, our ODE system breaks down. To force it to stay well behaved, we impose regularity conditions as boundary conditions. It will be sufficient to force the derivative of the radial velocity to behave correctly, we substitute the energy equation (76) into the radial momentum conservation equation (61) and rearrange to attain a differential equation for $\frac{dv_R}{dR}$.

$$\left(\frac{2\gamma}{\gamma+1} - \frac{v_R^2}{c_s^2}\right)\frac{1}{v_R}\frac{dv_R}{dR} = \frac{R(\Omega_K^2 - \Omega^2)}{c_s^2} - \frac{2\gamma}{\gamma+1}\left(\frac{1}{R} - \frac{1}{\Omega_K}\frac{d\Omega_K}{dR}\right) - \frac{\gamma-1}{\gamma+1}\frac{f\alpha R}{v_R}\frac{d\Omega}{dR}. \tag{99}$$

Then, to force $\frac{dv_R}{dR}$ to stay well behaved, we impose that both sides of equation (99) are zero and attain

$$v_R^2 = \frac{2\gamma}{\gamma+1}c_s^2 \tag{100}$$

$$(\Omega_K^2 - \Omega^2)R = c_s^2\frac{2\gamma}{\gamma+1}\left(\frac{1}{R} - \frac{1}{\Omega_K}\frac{d\Omega_K}{dR}\right) + c_s^2\frac{\gamma-1}{\gamma+1}\frac{f\alpha R}{v_R}\frac{d\Omega}{dR}. \tag{101}$$

4 Numerical Approach

As we discussed in section 3.4, we use the shooting method to solve the boundary value problem [47, 48]. The shooting method requires two algorithms. The first algorithm is an ODE solver that solves an initial value problem. The second algorithm is a root-finder, which which takes the ODE solver and cleverly guesses values of R_s so that we find the correct value more quickly than if we searched by brute force.

4.1 Runge-Kutta Methods

Given a guess at R_s and initial data, we solve the ODE system using a "Runge-Kutta" algorithm. Before we define Runge-Kutta, let's first describe a simpler, similar, method. The definition of a derivative is

$$\frac{d}{dR}\vec{y}(R) = \lim_{h\to 0}\left[\frac{\vec{y}(R+h) - \vec{y}(R)}{h}\right]. \tag{102}$$

Or, alternatively, if h is sufficiently small,

$$\vec{y}(R+h) = \vec{y}(R) + h\frac{d\vec{y}}{dR}(R). \tag{103}$$

If we know $\vec{y}(R_0)$ and $\frac{d}{dR}\vec{y}(R_0)$, then we can use equation (103) to solve for $\vec{y}(R+h)$. Then, let $R_1 = R_0 + h$ and use equation (103) to solve for $\vec{y}(R_1+h)$. In this way, we can solve for $\vec{y}(R)$ for all $R > R_0$. This method is called the "forward Euler" method [48].

Runge-Kutta methods are more sophisticated. One can use a Taylor series expansion to define a more accurate iterative scheme that relies on higher-order derivatives, not just first derivatives. However, since we only have first derivative information, we simulate higher-order derivatives by evaluating the first derivative at a number of different values of R. Then, of course, the higher-order derivatives are finite differences of these evaluations [47, 48].

We use a fourth-order Runge-Kutta method—which means the method effectively incorporates the first four derivatives of a function—with adaptive step sizes: the 4(5) Runge-Kutta-Fehlberg method [51]. We use our own implementation, which can be found here: [52].

4.2 Integrating Inwards

Unfortunately, the Runge-Kutta method only integrates from small R to large R. Since we are integrating inwards, not outwards, we need to generate an analogous ODE system that goes from R_{out} to R_s and not

the other way around. To do this, we define some new variables. Let

$$\tau = \frac{R - R_{out}}{R_s - R_{out}} \tag{104}$$

$$= \frac{R - 10^5 R_s}{R_s(1 - 10^5)}, \tag{105}$$

so that

$$R(\tau) = R_{out} + (R_s - R_{out})\tau \tag{106}$$

$$= R_s \left[10^5 + (1 - 10^5)\tau\right]. \tag{107}$$

$R(\tau = 0) = R_{out}$ and $R(\tau = 1) = R_s$. And let $\vec{z}$ such that

$$\frac{d}{dR}\vec{z} = -\vec{O}(z, \tau), \tag{108}$$

where $\vec{O}$ is the vector-valued function in equation (88). Now, to integrate inwards from R_{out} we solve the system in equation (108) by integrating upwards from $\tau = 0$. Then, for a given R, we can find $\tau(R)$ and plug it into $\vec{z}$. The result should be $\vec{y}(R)$, where $\vec{y}$ is the vector of variables we care about from equation (87).

4.3 Root Finding

For root finding, we use the bisection algorithm [48]. First, we test whether the left-hand sides of equations (100) and (101) are positive or negative. Assume without loss of generality that they are positive. If they're negative, then multiply the equations by -1.

We bound R_s between a maximum value and a minimum value. Call them R_{max} and R_{min}. Then we guess that R_s is exactly between these two values and integrate inward from R_{out} to our guessed R_s, call it R_g. If the left-hand sides of equations (100) and (101) are positive, we chose too large of a value for R_s. We let R_g be the new R_{max} and repeat. If they're negative, we chose too small of a value for R_s. We let R_g be the new R_{min} and repeat. Eventually we will converge on the correct value.

4.4 Testing The Implementation

To actually solve the system derived in section 3, we implement the shooting method with a 4(5) Runge-Kutta-Fehlberg integrator as the initial-value solver and with the bisection method as the root-finding algorithm [47, 48]. We implement both tools in C++ from scratch. We chose C++ because, even though it contains modern programming tools such as object-oriented and functional paradigms, it is extremely fast, often performing within a factor of 2 more CPU cycles than C [53].[12]

We implemented and tested the Runge-Kutta initial-value solver separately. The code is open-sourced and the implementation and unit tests can be found online at [52]. In addition, we tested the algorithm by using it as the time-stepping component in a simple (1+1)-dimensional wave equation solver, using the method of lines (for more information, see e.g., [48]). This test can also be found online at [55]. We tested the implementation of the root solver and the shooting method less intensely since these tools are less sophisticated.[13] The implementation of the entire algorithm and a few simple tests can be found at [56]. To convince you that the algorithm functioned correctly, we now briefly describe some of the tests performed and their significance.

[12] It is important to take numerical benchmarks with a grain of salt. Optimization and the skill of the programmer are substantially larger factors in code performance [54].

[13] We tested the root solver on a simple polynomial and found it to behave as expected.

4.4.1 High-Order One Point Integration

A fourth-order Taylor series method should be able to solve the initial value problem

$$\begin{cases} \frac{d^4y}{dt^4} = C_4 \ \forall \ t \in \mathbb{R} \\ \left.\frac{d^3y}{dt^3}\right|_{t=0} = C_3 \\ \left.\frac{d^2y}{dt^2}\right|_{t=0} = C_2 \\ \left.\frac{dy}{dt}\right|_{t=0} = C_1 \\ y(t=0) = C_0, \end{cases} \qquad \text{where } C_i = \text{constant } \forall \ i \in \{0,1,2,3,4\} \tag{109}$$

in a single computer time step. This is because an equation like (109) contains only fourth-order information. Similarly, a fifth-order Taylor series method should be able to solve a sufficiently simple initial value problem in a single time step.

To test our method, We performed this test on the fourth-order integration and the fifth-order error estimation pieces of our Runge-Kutta-Fehlberg method and found discrepancy on the order of machine epsilon, the round-off error inherent in the discretization of the real number line. Figure 4 shows the results of one such integration test. If the reader is so inclined, they can find this test in the unit test driver in [52].

4.4.2 A Simple Stability Test

As a simple test of stability, we use the Runge-Kutta initial-value solver to solve the 2^{nd}-order ODE system

$$\frac{d^2y(t)}{dt^2} = -y(t) \text{ with } \begin{cases} y(0) = 0 \\ y'(0) = 1 \end{cases} . \tag{110}$$

The solution to this problem is naturally

$$y(t) = \sin(t). \tag{111}$$

Figure 5 shows a typical high-accuracy integration of this equation and compares it to the expected value. An oscillatory solution is a good test of the stability of a Taylor-series method because the Taylor series always has non-zero higher-order terms that are not captured. And thus error builds up from truncating the Taylor series. Moreover, we roughly estimate the buildup of error by summing up the difference between a fourth-order and a fifth-order approximation at each time step. If the actual measured error is less than this, we're in very good shape. To investigate this, we require a very low error tolerance of the integrator and measure its deviation based on local truncation error. Figure 4.4.2 shows the results.

5 Results

In the attempted simulations we assume the following parameters:

$$\begin{aligned} M = 10M_\odot \qquad & a_* = 0 \\ f = 3.5 \times 10^{-5} \qquad & \alpha = 0.1 \\ \gamma = 1.5 \quad & \dot{M} = -(0.11)\tfrac{4\pi GMm_p}{(1-f)c\sigma_T}, \end{aligned} \tag{112}$$

where $\dot{M}$ is 11% the Eddington accretion rate, σ_T is the Thomson scattering cross-section, and m_p is the mass of a proton.

Unfortunately, the shooting method never correctly determined the sonic radius. In figures 7 and 8, we plot the regularization conditions (100) and (101) at the guessed "sonic point" after guessing a sonic radius

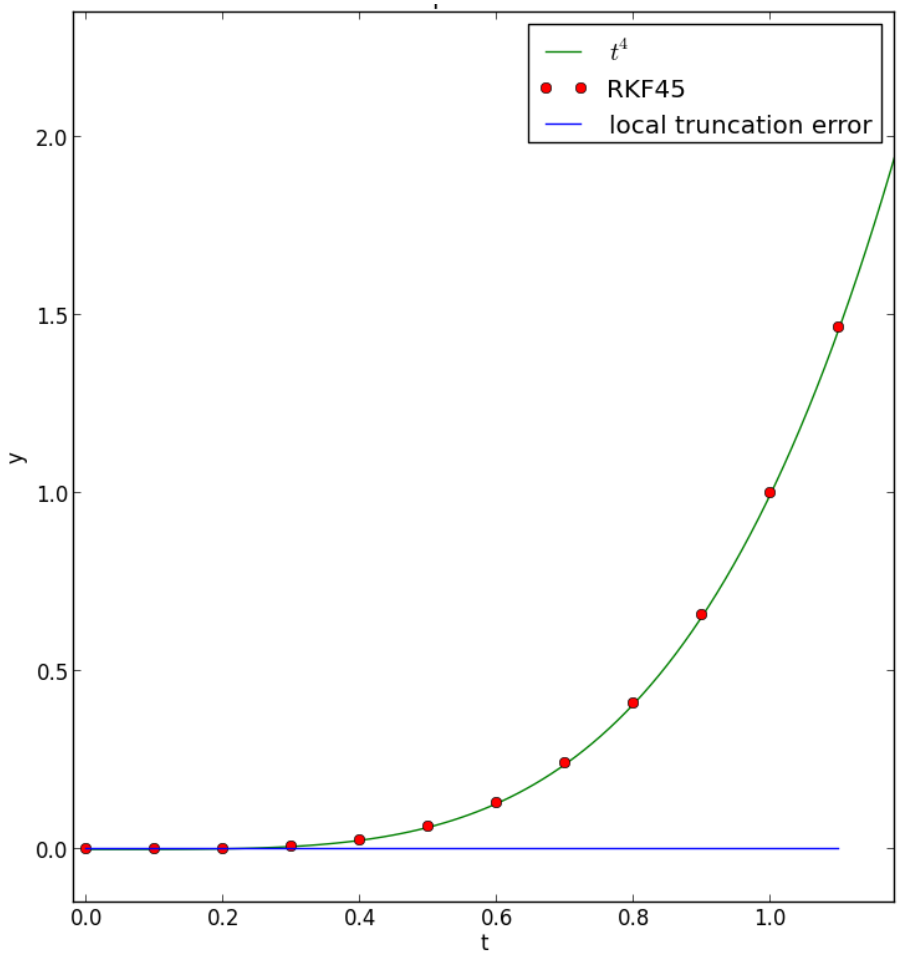

Figure 4: 4(5) Runge-Kutta Method for a Fourth-Order Polynomial. We demonstrate that our Runge-Kutta method is indeed a fourth-order Taylor series method by integrating a simple fourth-order initial value problem in a single computer time step. Each red dot is an integration starting at $t = 0$ to $t = x$. In each case, the result is a perfect x^4.

and integrating inwards. The conditions both diverge. Condition (7) diverges to $-\infty$ while condition (101) diverges to $+\infty$.

Surprisingly, these values line up perfectly with the values of the constraint equations evaluated on the self-similar solution described in section 3.4.1 at the guessed sonic radius. This indicates that the solution is not changing very much as we integrate from the outer boundary, and indeed a direct examination of the integration data confirms this. This static behavior is in direct contradiction with Shafee et al., who predict significant changes in every variable.

We suspect that the difficulty arises from integrating inwards from the outer boundary as opposed to outwards from the sonic point. Although it is not at all obvious, when the sonic point regularity conditions are true, equations (77), (78), and (79) become indeterminate and read $0/0$. In practice, sufficiently close to the sonic point, this might cause the numerical algorithm to evaluate all derivatives as zero and prevent the system from evolving as it should. And until the sonic point is reached, the self-similar solution is just that, self-similar. It doesn't change much anyway.

It might be possible to salvage the shooing method by using equation (63) at the outer boundary to

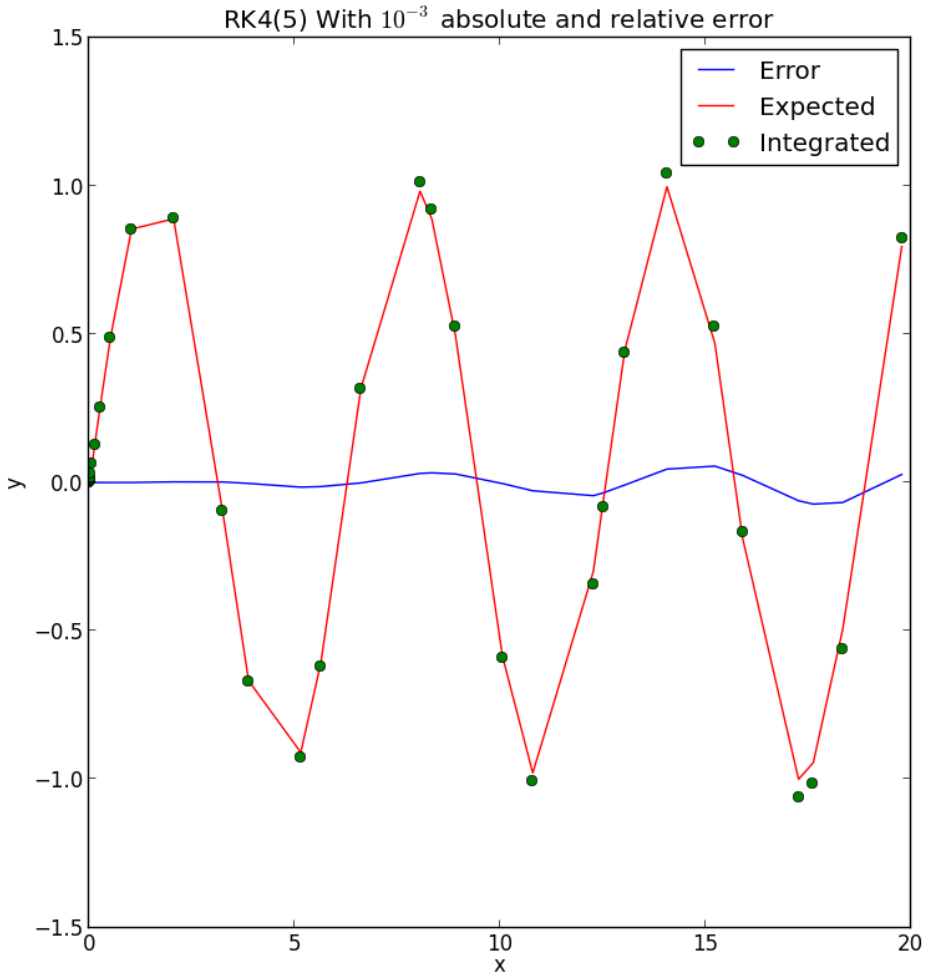

Figure 5: A high-order integration of equation (110) compared to the analytic solution. Over time, even a high-accuracy solution slowly diverges because the higher-order terms of the Taylor series are never zero.

calculate the integration constant j:

$$j = \Omega(R_{out})R_{out}^2 + \frac{\alpha c_s^2(R_{out})R}{v_R(R_{out})}. \tag{113}$$

Then, since j is constant, use (63) and the regularity conditions (100) and (101) to solve for initial data at the sonic point and integrate outwards instead of inwards. Unfortunately, the resulting system of algebraic equations is highly-nonlinear and must be solved numerically. In dimensions greater than one, root-finding methods for nonlinear systems of equations are very slow and unreliable [47, 48], and using the shooting method to integrate outwards implies running a root-finding algorithm for every single guess of R_s. This seemed very inefficient, which was why we didn't attempt it in the first place.

Shafee et al. didn't use the shooting method. Instead, they used a class of methods called "relaxation methods," [1] wherein one iteratively chooses a discretization for the ODE system that matches the boundary

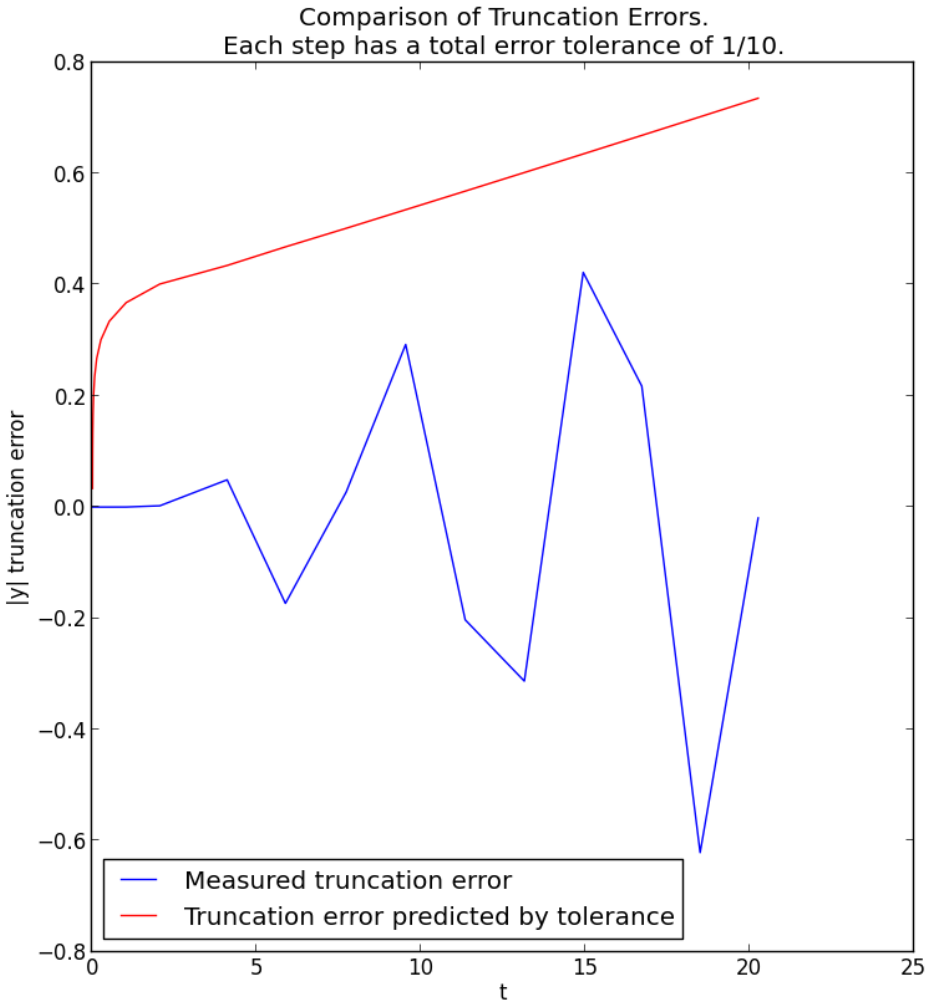

Figure 6: A low-order comparison of total error buildup as expected by the local truncation error compared to the actual measured deviation from the analytic solution. The total error is well within tolerance.

conditions [47]. In retrospect, it is likely that Shafee and collaborators predicted that the shooting method would be too naive. In a future attempt to generate a physically meaningful solution, we recommend the use of a dedicated boundary-value solver algorithm like a relaxation method.

6 Summary and Discussion

In summary, we were able to reproduce the analytic calculations of Shafee et al. [1] starting from Shakura and Sunyaev in 1973 [19] and working our way forwards through the history of axisymmetric accretion disks with effective viscosity [32, 33, 34, 35, 36, 37, 38, 39, 40, 41, 50]. For the fluid dynamics equations, We use the α prescription of Shakura and Sunyaev [19], the pseudo-Newtonian gravitational potentials of Mukopadhyay [42] and Paczynski and Wiita [43]. For the boundary data, we regularize the ODE system at the sonic

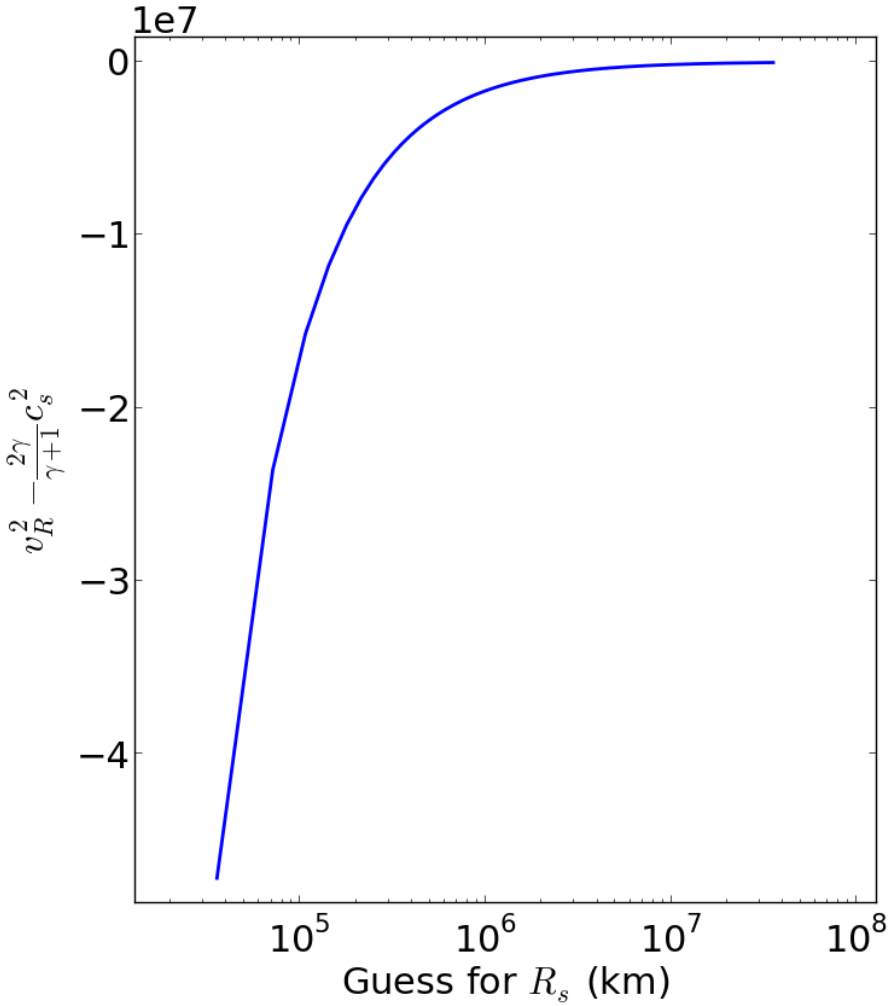

Figure 7: Evaluation of the regularization condition (100) at the guessed "sonic point" after integrating inwards from the outer boundary. The condition should evaluate to zero at the sonic point. However, it instead diverges to $-\infty$. The units on the y-axis are m^2/s^2.

point according to Shafee et al.'s method [1] and we impose self-similarity conditions at the outer boundary, according to Spruit et al. [49] and Narayan et al, [39].

We attempt to solve the resulting first-order ODE system by using the shooting method and integrating inwards from the outer boundary using a Runge-Kutta integrator. We are able to demonstrate the accuracy and stability of our numerical toolbox. However, the integration fails and remains mostly static and self-similar. We believe the problem stems from how the regularization conditions at the sonic point interact with the Runge-Kutta integrator. Therefore, a future attempt must either solve the regularization conditions to attain initial data integrate outwards or use a dedicated boundary-value problem solving tool such as a relaxation methods algorithm.

Although we failed to reproduce Shafee et al.'s results, we feel that this work is a valuable exploration of the methods in and history of accretion disk physics and offers valuable insight into which numerical

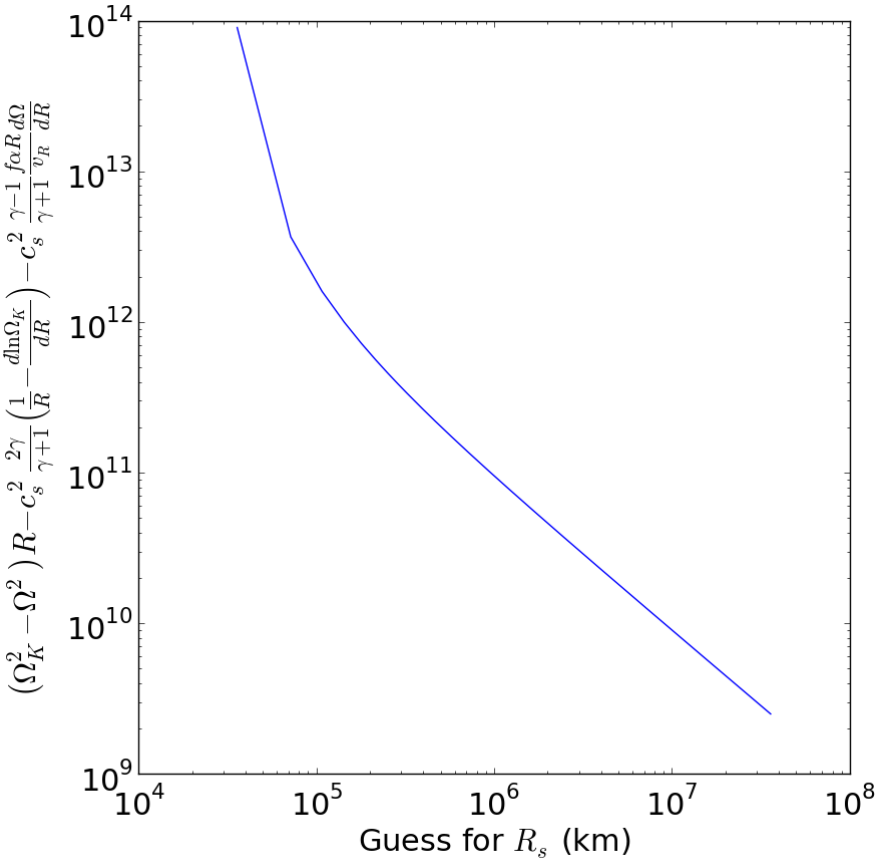

Figure 8: Evaluation of the regularization condition (101) at the guessed "sonic point" after integrating inwards from the outer boundary. The condition should evaluate to zero at the sonic point. However, it instead diverges to $+\infty$. The units on the y-axis are m/s^2.

approaches are appropriate for this sort of problem.

7 Acknowledgments

I would like to thank Professor Erik Schnetter for his advice on numerical methods and for understanding my time constraints. I'd also like to thank Scott VanBommel and Katherine White for many helpful discussions. Finally, I'd like to thank Professor Niayesh Afshordi for a fun, educational semester, and for assigning this challenging and interesting project.

A Demonstration that $H \approx c_s/\Omega_K$

Assume an axisymmetric thin disk orbiting around a central Newtonian compact object. Let the object have mass M and let the radial distance from the central object be R. Let the height above the plane of rotation be H. Let the vector pointing out from the central object be $\vec{r}$. This vector can be decomposed

into a radially outward component and a vertical component as follows

$$\vec{r} = R\hat{R} + z\vec{z}, \tag{114}$$

where $\hat{R}$ is the radial direction outward and $\hat{z}$ is the direction out of the plane of rotation.

The vertical component of the gravitational field due to the star is

$$g_z = -g_* \sin(\theta) = -\frac{GM}{r^2}\sin(\theta), \tag{115}$$

where θ is the angle between $\hat{r}$ and the orbital plane and g_* is the full gravitational field due to the star[20]. For a thin disk confined to roughly a single orbital radius ($r \approx R$ and $\theta << 1$),

$$g_z = -\frac{GM}{R^3}z. \tag{116}$$

But if the disk is in a circular orbit (and it should circularize), then it has Keplerian angular velocity [20]

$$\Omega_K = -\sqrt{\frac{GM}{R^3}}. \tag{117}$$

So,

$$g_z = -\Omega_K^2 z. \tag{118}$$

If we assume hydrostatic equilibrium, we have Euler's equation

$$\begin{aligned} \frac{d\vec{u}}{dt} &= \frac{1}{\rho}\vec{\nabla}P + \vec{\nabla}\Phi = 0, & (119)\\ \Rightarrow \frac{1}{\rho}\vec{\nabla}P &= -\vec{\nabla}\Phi = g & (120) \end{aligned}$$

where $\vec{u}$ is the velocity vector field, ρ is the density of the disk, P is the pressure of the disk, and Φ is the gravitational potential [9, 15]. If we confine ourselves to the z direction, this gives us that

$$\frac{1}{\rho}\frac{dp}{dz} = -\Omega_K^2 z. \tag{121}$$

Now, recall that the speed of sound c_s is defined by (21) as

$$P = c_s^2 \rho. \tag{122}$$

Then

$$\frac{1}{\rho}\frac{dP}{dz} = \frac{c_s^2}{\rho}\frac{d\rho}{dz}. \tag{123}$$

Then we have

$$\begin{aligned} \frac{c_s^2}{\rho}\frac{d\rho}{dz} &= -\Omega_K^2 z & (124)\\ \Rightarrow c_s^2 \int_{\rho_0}^{\rho_H} \frac{1}{\rho'} d\rho' &= -\Omega_K^2 \int_0^H z dz & (125)\\ \Rightarrow c_s^2 \ln\left(\frac{\rho_0}{\rho_H}\right) &= \frac{1}{2}\Omega_K^2 H^2 & (126)\\ \Rightarrow \frac{c_s}{H} &= \Omega_K \left[2\ln\left(\frac{\rho_0}{\rho_H}\right)\right]^{-1/2}, & (127) \end{aligned}$$

where ρ_H is the density at height H and ρ_0 is the density at the orbital plane. Of course, $\ln(x)$ grows incredibly slowly, and $\sqrt{\ln(x)}$ grows equally slowly. So the ln term is of order 1 and, for a rough approximation, we can safely neglect it:

$$H \approx \frac{c_s}{\Omega_K}. \tag{128}$$

References

[1] R. Shafee et al. Viscous torque and dissipation in the inner regions of a thin accretion disk: Implications for measuring black hole spin. *The Astrophysical Journal*, 676:549–561, March 2008.

[2] R. M. Wald. *General Relativity*. The University of Chicago Press, 1984.

[3] S. W. Hawking and G. F. R. Ellis. *The Large Scale Structure of Space-Time*. Cambridge University Press, 1973.

[4] J. McClintock et al. The spin of the near-extreme kerr black hole grs 195+105. *The Astrophysical Journal*, 652:518–539, November 2006.

[5] J. Liu et al. Precise measurement of the spin parameter of the stellar-mass black hole m33 x-7. *The Astrophysical Journal*, 679:L37–L40, May 2008.

[6] L. Gou et al. A determination of the spin of the black hole primary in lmc x-1. *The Astrophysical Journal*, 701:1076–1090, August 2009.

[7] J. Frank et al. *Accretion Power in Astrophysics*. Cambridge University Press, 2002.

[8] T. Padmanabhan. *Theoretical Astrophysics Volume 1: Astrophysical Processes*. Cambridge University Press, 2000.

[9] F. Melia. *High-Energy Astrophysics*. Princeton University Press, 2009.

[10] C. W. Misner et al. *Gravitation*. W.H. Freeman and Company, 1973.

[11] L. Lehner. Numerical relativity: A review. *Classical and Quantum Gravity*, 18:R25–R86, 2001.

[12] C. D. Ott et al. A case study for petascale applications in astrophysics: Simulating gamma-ray bursts. In *Proceedings of the 15th ACM Mardi Gras Conference*, MG '08, pages 18:1–18:9, New York, NY, USA, 2008. ACM.

[13] J. A. Font. Numerical hydrodynamics and magnetohydrodynamics in general relativity. *Living Reviews in Relativity*, 11(7), 2008.

[14] N. Bucciantini and L. Zanna. A fully covariant mean-field dynamo closure for numerical 3+1 resistive grmhd. *Montly Notices of the Royal Astronomical Society*, 428:71–85, 2013.

[15] M. J. Thompson. *An Introduction to Astrophysical Fluid Dynamics*. Imperial College Press, 2006.

[16] Wikipedia. Navierstokes equations — wikipedia, the free encyclopedia, 2013.

[17] Wikipedia. Fluid dynamics — wikipedia, the free encyclopedia, 2013.

[18] Wikipedia. Speed of sound — wikipedia, the free encyclopedia, 2013.

[19] N.I. Shakura and R.A. Sunyaev. Black holes in binary systems. observational appearance. *Astronomy and Astrophysics*, 24:337–355, 1973.

[20] S. T. Thorton and J. B. Marion. *Classical Dynamics of Particles and Systems*. Thomson Books, 2004.

[21] S. VanBommel. Simulation of turbulence in 2d shearing sheet keplerian accretion disks. *Niayesh Afshordi's Astrophysics Class*, 1(1), 2013.

[22] S. A. Balbus and J. F. Hawley. A powerful local shear instability in weakly magnetized disks. i. linear analysis. *The Astrophysical Journal*, 376:214–222, July 1991.

[23] J.F. Hawley and S.A. Balbus. A powerful local shear instability in weakly magnetized disks. ii. nonlinear evolution. *The Astrophysical Journal*, 376:223–233, July 1991.

[24] J.F. Hawley and S.A. Balbus. A powerful local shear instability in weakly magnetized disks. iii. long-term evolution in a shearing sheet. *The Astrophysical Journal*, 400(2):595–609, 1992.

[25] J.F. Hawley and S.A. Balbus. A powerful local shear instability in weakly magnetized disks. iv. nonaxisymmetric perturbations. *The Astrophysical Journal*, 400:610–621, 1992.

[26] J. F. Hawley et al. Local three-dimensional magnetohydrodynamic simulations of accretion disks. *The Astrophysical Journal*, 440:742–763, February 1995.

[27] J. F. Hawley et al. Local three-dimensional simulations of an accretion disk hydromagnetic dynamo. *The Astrophysical Journal*, 464:690–703, June 1996.

[28] J. R. Taylor et al. *Modern Physics for Scientists and Engineers*. Prentice Hall, Inc., 2004.

[29] S. N. Zhang et al. Black hole spin in x-ray binaries: Observational consequences. *The Astrophysical Journal*, 482:L155–L158, June 1997.

[30] R. Shafee et al. Estimating the spin of stellar-mass black holes by spectral fitting of the x-ray continuum. *The Astrophysical Journal*, 636:L113–L116, January 2006.

[31] S. W. Davis et al. Relativistic accretion disk models of high-state black hole x-ray binary spectra. *The Astrophysical Journal*, 621:372–387, March 2005.

[32] B. Paczynski and G. Bisnovatyi-Kogan. A model of a thin accretion disk around a black hole. *Acta Astronomica*, 31(3):283–291, 1981.

[33] B. Mochotrzeb and B. Paczynski. Transonic accretion flow in a thin disk around a black hole. *Acta Astronomica*, 32.1(2):1–11, 1982.

[34] S. Kato et al. Pulsational instability of transonic regions of accretion disks with conventional α-viscosity. *Publications of the Astronomical Society of Japan*, 40:709–727, 1988.

[35] M.A. Abramowicz et al. Slim accretion disks. *The Astrophysical Journal*, 332:646–658, September 1988.

[36] R. Popham and R. Narayan. Does accretion cease when a star approaches breakup? *The Astrophysical Journal*, 370:604–614, April 1991.

[37] R. Narayan and R. Popham. Hard x-rays from accretion disk boundary layers. *Nature*, 362:820–822, April 1993.

[38] X. Chen and R. Taam. The structure and stability of transonic accretion disks surrounding black holes. *The Astrophysical Journal*, 412:254–266, July 1993.

[39] R. Narayan et al. Global structure and dynamics of advection-dominated accretion flows around black holes. *The Astrophysical Journal*, 476:49–60, February 1997.

[40] X. Chen et al. Advection-dominated accretion: Global transonic solutions. *The Astrophysical Journal*, 476:61–69, February 1997.

[41] N. Afshordi and B. Paczynski. Geometrically thin disk accreting into a black hole. *The Astrophysical Journal*, 592:354–367, July 2003.

[42] B. Mukhopadhyay. Description of pseudo-newtonian potential for the relativistic accretion disks around kerr black holes. *The Astrophysical Journal*, 581:427–430, December 2002.

[43] B. Paczynsky and P.J. Wiita. Thick accretion disks and supercritical luminosities. *Astronomy and Astrophysics*, 88:23–31, 1980.

[44] R. Penna. Simulations of magnetized discs around black holes: Effects of black hole spin, disc thickness, and magnetic field geometry. *Monthly Notices of the Royal Astronomical Society*, 408:752–782, 2010.

[45] R. Penna. *Black Hole Accretion Disks and Jets: Connecting Simulations and Theory*. PhD thesis, Harvard University, 2013. `http://nrs.harvard.edu/urn-3:HUL.InstRepos:11108714`.

[46] D. V. Schroeder. *Thermal Physics*. Addison Wesley Longman, 2000.

[47] W. H. Prss et al. *Numerical Recipes: The Art of Scientific Computing. Third Edition.* Cambridge University Press, 2007.

[48] M. T. Heath. *Scientific Computing: An Introductory Survey*. McGraw-Hill, 1997.

[49] H. C. Spruit et al. Spiral shocks and accretion in discs. *Monthly Notices of the Astronomical Society*, 229:517–527, June 1987.

[50] R. Narayan and I. Yi. Advection-dominated accretion: A self-similar solution. *The Astrophysical Journal*, 428(L13), 1994.

[51] E. Fehlberg. Klassische runge-kutta-formeln vierter und niedrigerer ordnung mit schrittweiten-kontrolle und ihre anwendung auf wrmeleitungsprobleme. *Computing*, 6(1-2):61–71, 1970.

[52] J. M. Miller. Runge-kutta in c++, 2013. `https://github.com/Yurlungur/runge_kutta`.

[53] The Open Source Community. The benchmarks game. `http://benchmarksgame.alioth.debian.org/`.

[54] Todd Mytkowicz et al. Producing wrong data without doing anything obviously wrong. In *In Proc. of Intl Conf. on Architectural Support for Programming Languages and Operating Systems*, pages 265–276. ACM, 2009.

[55] J. M. Miller. (1+1)-dimensional wave equation solver in c++, 2013. `https://github.com/Yurlungur/wave_equation`.

[56] J. M. Miller. Shooting method for accretion discs in c++, 2013. `https://github.com/Yurlungur/accretion_spectrum`.